Biochemical and Biophysical Research Communications 373 (2008) 69–73

Contents lists available at ScienceDirect

Biochemical and Biophysical Research Communications

journal homepage: www.elsevier.com/locate/ybbrc

Direct evidence of vinculin tail–lipid membrane interaction in beta-sheet conformation

Gerold Diez [a], Felix List [b], James Smith [c], Wolfgang H. Ziegler [d], Wolfgang H. Goldmann [a,*]

[a] Center for Medical Physics and Technology, Biophysics Group, Friedrich-Alexander-University of Erlangen-Nuremberg, Henke strasse 91, Erlangen, Germany
[b] Institute of Biophysics and Physical Biochemistry, University of Regensburg, Germany
[c] School of Engineering and Science, Jacobs University Bremen, Germany
[d] IZKF Leipzig, Faculty of Medicine, University of Leipzig, Germany

ARTICLE INFO

Article history:
Received 21 May 2008
Available online 11 June 2008

Keywords:
Vinculin
Vinculin tail carboxy-terminal peptide
Lipid membrane binding
Focal adhesion complex
Molecular dynamics simulation
Differential scanning calorimetry
Circular dichroism spectroscopy

ABSTRACT

The focal adhesion protein vinculin (1066 residues) plays an important role in cell adhesion and migration. The interaction between vinculin and lipid membranes is necessary to ensure these processes. There are three putative lipid-membrane interaction sites located at the vinculin tail domain two that form amphipathic alpha-helices (residues 935–978 and 1020–1040) and one that remains unstructured (residues 1052–1066) during crystallization. In this work, the structural and biochemical properties of the last 21 residues of the vinculin tail domain were investigated. Differential scanning calorimetry was performed in the presence of lipid vesicles consisting of dimyristoyl-L-α-phosphatidylcholine and dimyristoyl-L-α-phosphatidylglycerol at various molar ratios. The results demonstrate that this peptide inserts into lipid vesicle membranes. Examining the secondary structure of this peptide by molecular dynamics simulations and circular dichroism spectroscopy, we show that it adopts an antiparallel beta sheet backbone geometry that could ensure the association with lipid vesicles.

Cell adhesion and cell–cell contacts are important for cell survival and proliferation. Adhesion processes are driven by extra cellular matrix (ECM) contacts that trigger biochemical as well as biomechanical signals inside the cells [1,2]. The focal adhesion complex (FAC) that links the ECM *via* integrins with the actin cytoskeleton of the cell is involved in these processes. It consists of many proteins that control biochemical signaling and cytoskeletal dynamics, which include talin, zyxin, paxillin, focal adhesion kinase (FAK) and vinculin [3]. Some of these proteins are believed to interact transiently with the lipid membrane [4]. However, the nature and cellular function of these interactions are poorly understood [5,6].

Vinculin is one of the FAC proteins that shows *in vitro* and *in vivo* lipid-binding capabilities [7–12]. Cleavage of vinculin with proteaseV8 separates the protein into a 95 kDa (residues 1–858) head and a 30 kDa (residues 858–1066) tail fragment [13]. Under physiological ionic conditions, the tail domain can associate with phosphatidylinositol (PI) vesicles whilst the head shows no lipid interaction [9]. In the activated or open conformation of vinculin, the head domain dissociates from the tail to unmask cryptic-binding sites for other FAC proteins such as paxillin, actin and lipids [14,15]. It has been demonstrated that talin and phospholipids both have the capability to displace the head from the tail domain to activate the vinculin molecule [15–17].

There are three regions on the 30 kDa tail domain that have been identified as candidates for lipid-binding: residues 935–978, 1020–1040, and 1052–1066 [10,11,18]. The entire vinculin tail (Vt) consists of a bundle of five alpha-helices followed by a C-terminal arm that remained unstructured during crystallization and can be divided into three different parts: a flexible loop (residues 1047–1052), a beta-clamp (residues 1053–1061) and a hydrophobic hairpin (residues 1062–1066). Parts of this C-terminal arm (residues 1052–1066) are known to influence the membrane binding of vinculin [11,12]. Pull-down assays with artificial lipid membranes consisting of phosphatidylserine (PS) or a mixture of 40% phosphatidylinositol-4,5-bisphosphate (PIP_2) and 60% phosphatidylcholine (PC) revealed that in contrast to Vt, a variant lacking the last 15 amino acids (VtΔC), does not interact with vesicles of these compositions [11,12]. To what extent the last 15 residues are involved in lipid interaction was not determined.

This study explores and characterizes the lipid-binding ability of the C-terminal arm which includes the last 15 residues of vinculin using differential scanning calorimetry (DSC). Results demonstrate that the C-terminal arm is directly involved in lipid binding and can insert into the lipid vesicle consisting of DMPC/DMPG at various molar ratios. The secondary structure of the C-terminal arm was also explored using molecular dynamics simula-

* Corresponding author. Fax: +49 9131 85 25601.
E-mail address: wgoldmann@biomed.uni-erlangen.de (W.H. Goldmann).

0006-291X/$ - see front matter © 2008 Elsevier Inc. All rights reserved.
doi:10.1016/j.bbrc.2008.05.182

tions which predicted an antiparallel beta-sheet followed by an unstructured C-terminal end. This conformational behavior was further explored in the presence/absence of DMPC/DMPG vesicles using CD-spectroscopy. The results suggest direct association of vinculin's lipid-binding region (residues 1052–1066) with membranes whilst forming a beta-sheet.

Materials and methods

Peptide and lipid preparations. The last 21 residues of the vinculin tail domain are IKIRTDAGFTLRWVRKTPWYQ. This peptide was synthesized by Dr. Sven Rothemund (IZKF, Leipzig). Prior to calorimetric measurements, the peptide was dissolved in a buffer containing 20 mM HEPES (pH 7.4), 2 mM EDTA, 5 mM NaCl and 0.2 mM DTT. For CD-spectroscopic measurements, the peptide was dissolved in 10 mM potassium phosphate buffer at pH 7.4.

Multilamellar vesicles (MLVs) were prepared from dimyristoyl-L-α-phosphatidylcholine (DMPC) and dimyristoyl-L-α-phosphatidylglycerol (DMPG) (Avanti Polar Lipids, Birmingham, AL, USA). Mixtures of crystalline DMPC and DMPG were dissolved in chloroform/methanol at 2:1 (v/v) and the solvent was evaporated under a stream of nitrogen to form a dry lipid film on the glass wall. This was followed by a further 2 h vacuum desiccation. For calorimetric measurements, the lipid film was suspended in above buffer and left overnight at 35 °C for multilamellar vesicle formation. For CD-spectroscopic experiments, small unilamellar vesicles (SUVs) were used; for that the lipid film was dissolved in 10 mM potassium phosphate buffer at pH 7.4 and then sonicated.

Differential scanning calorimetry (DSC). A differential scanning calorimeter Q100 (TA Instruments) was used and the pure MLV solution was placed in the reference cell and the MLV-peptide solution in the sample cell. Under sealed conditions, both solutions were heated at a rate of 0.5 °C/min and cooled at 1 °C/min. The heat capacity was recorded between +7 and +30 °C until the equilibrium of the phase transition enthalpy was reached. The phase transition peak was observed at around 23 °C. Purified insulin (purchased from Sigma–Aldrich) was used as a control peptide.

Molecular dynamics (MD) simulation. The last 20 residues of chicken vinculin (RCSB Protein Data Bank, http://www.pdb.org; crystal 1ST6) were used as a starting geometry for all MD-simulations. The terminal residue of the sequence, glutamine (Gln, Q), was added by the *Swissprot PDB viewer* (http://www.expasy.org/spdbv) to complete the sequence.

The simulations were performed with the GROMACS 3.3.1 package [19] running on a 4 core 2.2 GHz PC with 6.2GB RAM using GENTOO Linux. The MD simulation involved a 1.5 nm octahedron box filled with approximately 7850 spc216 water molecules under periodic boundary conditions [20]. To keep the net charge neutral during the simulations, additional chloride ions were added. The GROMACS force field ffG53a6 [21] was used and all bonds were constrained by applying LINCS [22]. Long-range electrostatics was handled by the Particle Mesh Ewald (PME) method. A non-bonded cut off of 0.9 nm for the Lennard-Jones potential was used. All simulations were performed in a pressure coupled Berendsen temperature bath at 300 K [23]. Energy minimization was performed using the Steepest Descent method. Prior to the simulations positional restraints were applied. The final MD-runs were performed at 2 fs time steps and conformational snapshots taken every 100 ps over 10,000 ps.

The secondary structure was calculated using the Dictionary of Protein Secondary Structure (DSSP) designed by Kabsch and Sanders [24]. Snapshots (1–100) were taken to generate a pair-wise difference Euclidian distance matrix using the available sixty dihedral angles. The difference between dihedrals ($\Delta\theta_{n,m}$) was defined as,

$$\Delta\theta_{n,m} = min\,(|\theta_{n,p} - \theta_{m,p}|,\ |\theta_{n,p} - \theta_{m,p} + 360^\circ|,\ |\theta_{m,p} - \theta_{n,p} - 360^\circ|),$$

where for any two structures n and m at a given dihedral angle p = 1 to 60. Ward's geometric minimal variance and agglomerative hierarchical clustering [25] was applied to each pair-wise difference distance matrix. The resulting dendogram was partitioned using Mojena's stopping rule number 1 [26] to identify significantly different clusters and, therefore, to represent distinct conformational groups.

Circular dichroism (CD spectroscopy). CD spectroscopy was performed on a JASCO J-815 CD spectrophotometer and measurements were taken between 180 and 260 nm and recorded at 1 nm intervals using a quartz cuvette of 0.1 cm path length. Three spectra of a 70 μM peptide solution at a P/L molar ratio of 1:40 were recorded and averaged.

CD spectra of the vinculin peptide were taken at 30 °C, smoothed and fitted by the Savitzky–Golay algorithm and secondary structure analysis was performed using the CONTINLL and CDSSTR algorithms provided by DICHROWEB [27,28]. The quality of fits between experimental and calculated spectra was assessed by normalized root mean square deviation (NRMSD, cf. Mao et al. 1982 Biochemistry 21:4690).

Results

Differential scanning calorimetry

The insertion of the vinculin peptide into artificial phospholipid membranes was determined using calorimetry. The measurements were performed with MLVs at 10 mg/ml consisting of DMPC/DMPG at various molar ratios. In Fig. 1A, MLVs at a molar ratio of 70:30 DMPC/DMPG were incubated with the 21 residue vinculin peptide and the specific heat was determined. With increasing peptide concentration (from 0 to 180 μM) the specific heat and phase transition temperature (T_m) of MLVs decreased compared to MLVs in the absence of vinculin peptide. The relative flattening of the curve together with the shift of T_m to lower temperatures are indicative for peptide insertion into lipid bilayers [29]. The decrease in relative transition enthalpy ($\Delta H/\Delta H_0$) as a function of increasing peptide concentration was plotted in Fig. 1B for DMPC/DMPG vesicles of different molar ratios. Increasing the concentration of negatively charged lipids in the vesicles causes a decrease in peptide-lipid insertion behavior. Insulin (control) showed no changes in relative transition enthalpy (Fig. 1B, blue line).

Molecular dynamics investigation

To elucidate the secondary structure of the C-terminal lipid-binding region of the vinculin tail domain, MD-simulations were performed in an explicit solvent and with counter ions. To ensure the reliability of results, the 10 ns simulation was performed three times. During the simulation, an antiparallel beta-sheet emerged after 3.5 ns. Residues 2–12 took part in the secondary structure element whilst residues 13–21 remained unstructured under the conditions of the simulation (Fig. 2A).

Conformational analyses were also performed to identify a representative structure (backbone geometry). The starting conformation (snapshot 0), at time t = 0 ps, was not used in the conformational analysis. The cluster analysis of the pairwise difference distance matrix derived from the dihedral angles ($\Delta\theta_{n,m}$ above) and from the snapshots 1 (at t = 100 ps) to 100 (at t = 10,000 ps) revealed statistically significant ($p < 0.05$) conformational clusters illustrated in red and black in the dendrogram (Fig. 2B). The representative geometry for each cluster is colored in green. Where the snapshot sequence appears to jump between clusters, the conformations are likely to be associated with a plateau (and are not at well-defined local minima) on a potential energy landscape.

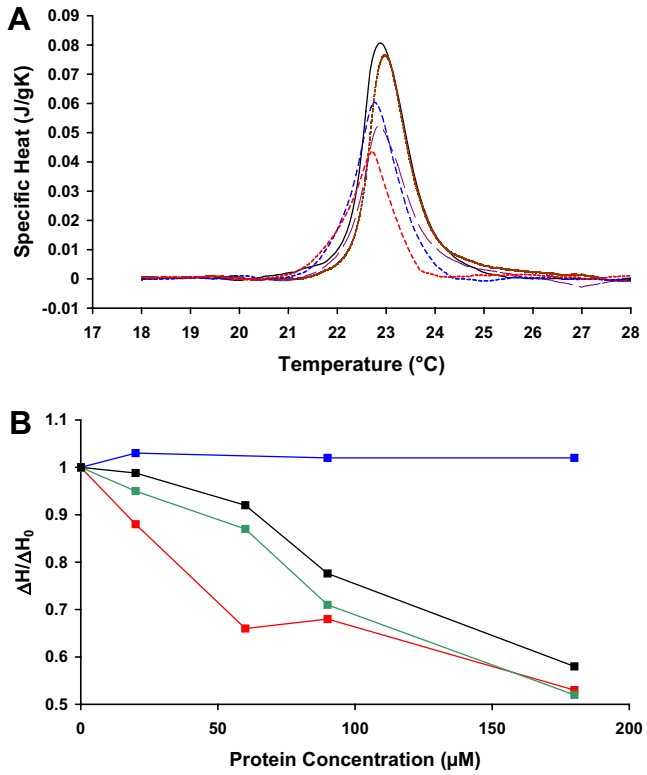

Fig. 1. Vinculin tail peptide interactions with MLVs. (A) Thermograms from DSC measurements with lipid vesicles containing DMPC and DMPG at a molar ratio of 70:30. The specific heat decreased with increasing peptide concentration. (—) Lipid only, (– – –) 20 μM, (– – –) 60 μM, (– – –) 90 μM, and (– – –) 180 μM peptide (n = 4–6 runs). Note, that the integral of the specific heat provides the phase transition enthalpy ΔH. (B) Relative phase transition enthalpy changes of DMPC/ DMPG vesicles at different molar ratios of DMPC/DMPG, 70:30 (——); DMPC/DMPG, 50:50 (——); DMPC/DMPG, 30:70 (—). With increasing vinculin peptide concentration the phase transition enthalpy decreased as a consequence of the lipid insertion of this peptide. (——) Indicates the phase transition enthalpy of insulin incubated with DMPC/DMPG vesicles of a molar ratio of 70:30. Note, there were no detectable changes in enthalpy under all lipid compositions for insulin (data not shown). (For interpretation of color mentioned in this figure the reader is referred to the web version of the article.)

The cluster labeled with an asterisk is the most densely packed and represents the energetically most favorable region. All the geometries in that group represent a beta-sheet conformation. The structure extracted at 8400 ps is the energetically most favorable and representative of the simulation (Fig. 2C). Examining the structure, the first six residues of the lipid-binding site (residues 1052–1057) are part of the turn and the second strand of the beta-sheet conformation. This clearly implicates the lipid-binding site of the vinculin C-terminus takes part in beta-sheet formation.

CD-spectroscopy

The secondary structure of the peptide in the presence/absence of SUVs was determined using CD-spectroscopic measurements. SUVs consisting of DMPC/DMPG at a molar ratio of 70:30 were used in these experiments. Measuring between 180 and 260 nm, the spectrum for pure peptide showed a minimum at 200 nm, whilst in the presence of SUVs this minimum was shifted to 223 nm (Fig. 3). This observation suggests a clear change in conformation of the peptide. Analyses of the spectral data using the algorithms (CDSSTR and CONTINLL), that employ different approaches for deconvoluting the CD data (cf. Lees et al. 2006 Bioinformatics, 22:1955) from a database of secondary structure contributions, show similar structural elements within the vinculin C-terminal peptide. CDSSTR shows 25% beta strand 1, 13% beta strand 2, 43% random coil (NRMSD < 0.016) and CONTINLL 21.9% beta strand 1, 13% beta strand 2, 42.6% random coil (NRMSD < 0.134). These analyses indicate a possible antiparallel beta-sheet conformation. It is reassuring that the CD spectrum of the peptide allows an interpretation which agrees with the representative at 8400 ps derived from the MD simulation.

In presence of SUVs, CD spectroscopy of the vinculin peptide provided similar results. In comparison to the spectra in the absence of lipid vesicles, the two algorithms indicate also two beta-strands and unstructured parts at a similar distribution (NRMSD < 0.05) for both CDSSTR and CONTINLL. However, the difference in spectral characteristics of the spectra for the peptide in the presence/absence of lipid vesicles suggests distinguishable beta-sheet conformations.

Discussion

Determining membrane binding characteristics of focal adhesion proteins is an important aspect in functional cell biology. Recent studies have shown that adhesion site dynamics, turnover and cell motility are directly affected by vinculin tail binding to phospholipids [12,30].

Two different strategies generating lipid-binding deficient vinculin mutants were examined: one approach was based on a variant lacking the last 15 residues of vinculin's C-terminus [12,30], whilst the other introduced six point-mutations on surface exposed basic residues to achieve a similar effect (on binding acidic phospholipid vesicles) *in vitro* [30]. It was reported that vinculin deficient in lipid binding still locates at focal adhesions, but that the FAC turnover was impaired [12,30]. Moreover, these studies showed that binding of the vinculin tail to lipid membranes is dependent on the capacity of vinculin to interact with acidic phospholipids, such as phosphatidylserine (PS) and phosphatidylinositol-4,5-bisphosphate (PIP_2). Work focussing on the possible involvement of acidic phospholipids in adhesion site turnover left the question unanswered of whether or not the vinculin tail C-terminal arm interacts directly with phospholipid membranes. To this end an investigation into the function of the C-terminal region was required as many studies had previously indicated that the C-terminus of the vinculin tail interacted with phospholipids such as phosphatidylcholine, phosphatidylserine as well as PIP_2 [10,11].

To gain information about the thermodynamic behavior of artificial lipids in the presence/absence of the 21-residue C-terminal peptide of the tail domain, we applied differential scanning calorimetry. Using MLVs allowed the detection of subtle perturbations during the lipid melting process and gave direct evidence of peptide–lipid interaction. As described in Fig. 1, the C-terminal peptide of vinculin showed membrane insertion behavior. Since membrane–protein interactions are known to depend on the negative surface charge of membranes, we increased the charge of lipid vesicles to mimic the inner leaflet of the cell membrane. The results showed that the phase transition enthalpy increased, suggesting reduced binding of vinculin's C-terminal region with the membrane (Fig. 1B). This result demonstrates that the lipid interaction of the C-terminal site is driven by the peptide's hydrophobic potential and not by acidic phospholipids. It is assumed that *in vivo* the C-terminal arm is exposed to the cytosolic environment and available even in the closed protein conformation. Therefore, the C-terminal arm may tether vinculin to the cell membrane and facilitate its interaction with focal adhesion complexes.

Site-directed mutagenesis revealed that intermolecular interactions between the vinculin tail and lipids are controlled by surface-exposed, basic residues [30]. Furthermore, a change of two resi-

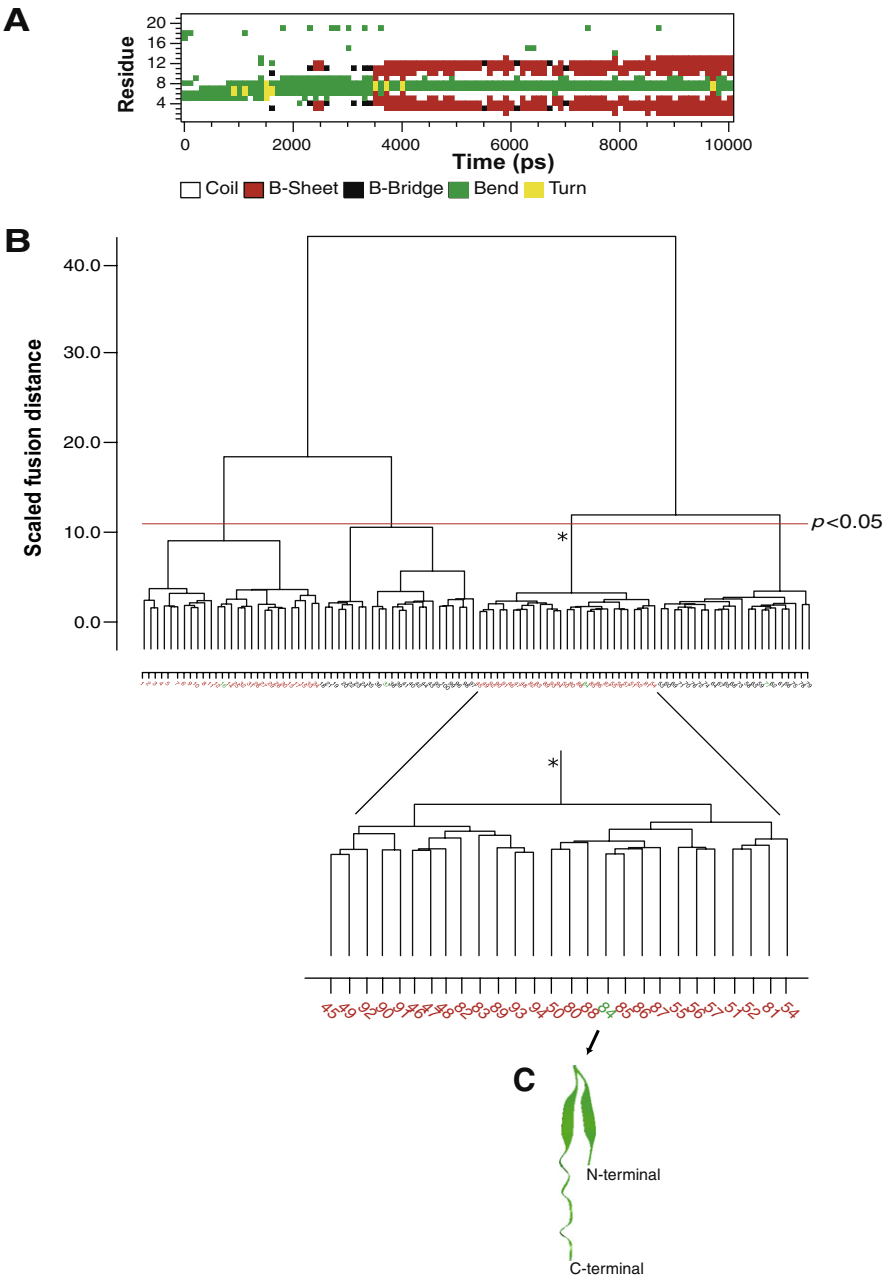

Fig. 2. (A) Emergent secondary structure of the C-terminal 21 residues of the C-terminal vinculin tail peptide under charge neutral conditions according to DSSP. (B) Clustered conformations of the 21 residue vinculin tail peptide. The scaled fusion distance is used for measuring the distance between any two fusions or clusters. The *x*-axis represents the snapshots taken during MD-simulations. The clusters are colored in black and red; the representative structure of each cluster is colored in green. Note, that the most compact cluster of the run is magnified. (C) The representative structure of the most compact cluster at time point 8400 ps. (For interpretation of color mentioned in this figure the reader is referred to the web version of the article.)

dues (R1060Q; K1061Q) located in the C-terminal lipid-binding site significantly impaired the interaction of vinculin tail with vesicles containing acidic phospholipids. DSC measurements using a 21-residue peptide carrying this mutation indicated, however, a higher lipid insertion potential for DMPC/DMPG vesicles (data not shown). Hence, changing residues from charged (R, K) to uncharged (Q, Q) increased the hydrophobic character of this peptide and resulted in increased interactions with moderately charged lipid vesicles. The increased hydrophobic moment of the C-terminal arm may also explain why the lipid binding of vinculin tail (R1060Q/K1061Q) was suppressed [30]. A conformational change in vinculin tail leading to a buried C-terminus may result in the loss of a membrane interaction site and reduced lipid binding.

The crystal structure of vinculin was determined at extremely low pH and at poorly solvated conditions [11,31]. Further, crystallization results in only one possible protein conformation which gives no information about flexible regions. We investigated the local conformational flexibility of the vinculin C-terminal peptide using MD-simulations. Our observations indicated that under nominally protonating (acidic) conditions, where the basic and acidic groups (excluding the amino-terminus) were protonated (basic residues, nominal +1 charge; acidic groups, including the terminus at charge 0), only unstructured conformations and no stable secondary structural elements emerged. This finding may explain why the C-terminal region (residue 1045–1066) remained unstructured in the crystal. However, under the normal (pH 7) con-

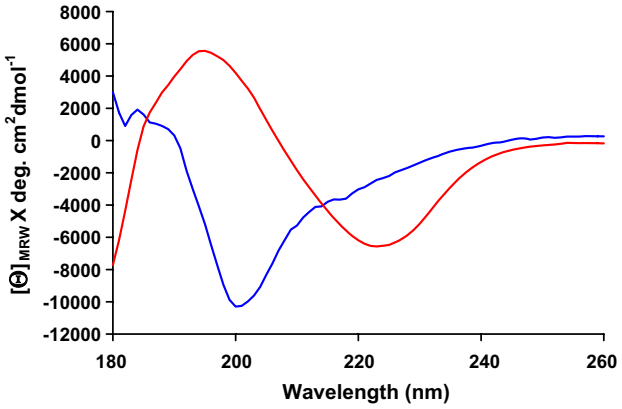

Fig. 3. Results from CD-spectroscopic measurements of the C-terminal peptide in the presence/absence of SUVs. The CD spectra of 70 μM peptide were obtained in10 mM sodium phosphate at pH 7.4 in the presence (——)/absence (——) of SUVs at 30 °C ($n = 3$). The values are expressed as mean residue molar ellipticity, Θ ($deg\,cm^2\,dmol^{-1}$). (For interpretation of color mentioned in this figure the reader is referred to the web version of the article.)

ditions of the MD-simulation, a more stable antiparallel beta-sheet emerged followed by a mostly unstructured C-terminus.

Further support for a secondary structure formation of the 21 residue peptide comes from CD spectroscopy and results indicate also beta-strands and unstructured parts of the C-terminal region. Together with results of the conformational analysis of the MD-simulation it allows an interpretation of the secondary structure of the C-terminal arm: (i) residues 2–6 form an initial beta-strand that represents the first part (residues 1045–1051) and (ii) residues 7–12 complete the beta-strand of the C-terminus of the tail domain (residues 1052–1057). The difference in spectral characteristics of the 21-residue peptide during CD spectroscopy in presence/absence of lipid vesicles can be explained by the high variance of beta-sheet structures. These could be due to parallel and antiparallel orientations and different twists which are reflected in different backbone angles [32].

In conclusion, this study indicates that the C-terminal 21 residues of the vinculin tail have clear lipid-binding potential. They have the capability to associate with, or indeed insert into, artificial lipid membranes probably by forming an antiparallel beta-sheet. Further detailed MD studies, exploring the conformational behavior of the full length vinculin-tail domain incorporating explicit pK_a/pK_d for the different protonation states of the charged residues, are clearly the next step in clarifying the essential interactions between different lipid molecules and the vinculin tail domain in focal adhesion complexes.

Acknowledgments

This work was funded by Deutsche Forschungsgemeinschaft, VolkswagenStiftung, NATO, BaCaTeC, and BFHZ. The authors thank Ben Fabry, Reinhard Sterner, Vitali Schewkunow, Martin Stiebritz, and Klaus-Jürgen Tiefenbach for their help and valuable discussions.

References

[1] B. Geiger, A. Bershadsky, Exploring the neighborhood: adhesion-coupled cell mechanosensors, Cell 110 (2002) 139–142.
[2] C.T. Mierke, P. Kollmannsberger, D. Paranhos-Zitterbart, J. Smith, B. Fabry, W.H. Goldmann, Mechano-coupling and regulation of contractility by the vinculin tail domain, Biophys. J. 94 (2008) 661–670.
[3] R. Zaidel-Bar, S. Itzkovitz, A. Ma'ayan, R. Iyengar, B. Geiger, Functional atlas of the integrin adhesome, Nat. Cell Biol. 9 (2007) 858–867.
[4] V. Niggli, S. Kaufmann, W.H. Goldmann, T. Weber, G. Isenberg, Identification of functional domains in the cytoskeletal protein talin, Eur. J. Biochem. 224 (1994) 951–957.
[5] V. Niggli, Structural properties of lipid-binding sites in cytoskeletal proteins, Trends Biochem. Sci. 26 (2001) 604–611.
[6] D.L. Scott, G. Diez, W.H. Goldmann, Protein–lipid interactions: correlation of a predictive algorithm for lipid-binding sites with three-dimensional structural data, Theor. Biol. Med. Modell. 3 (2006) 17.
[7] V. Niggli, L. Sommer, J. Brunner, M.M. Burger, Interaction in situ of the cytoskeletal protein vinculin with bilayers studied by introducing a photoactivatable fatty acid into living chicken embryo fibroblasts, Eur. J. Biochem. 187 (1990) 111–117.
[8] W.H. Goldmann, V. Niggli, S. Kaufmann, G. Isenberg, Probing actin and liposome interaction of talin and talin–vinculin complexes: a kinetic, thermodynamic and lipid labeling study, Biochemistry 31 (1992) 7665–7671.
[9] R.P. Johnson, S.W. Craig, The carboxy-terminal tail domain of vinculin contains a cryptic binding site for acidic phospholipids, Biochem. Biophys. Res. Commun. 210 (1995) 159–164.
[10] R.P. Johnson, V. Niggli, P. Durrer, S.W. Craig, A conserved motif in the tail domain of vinculin mediates association with and insertion into acidic phospholipid bilayers, Biochemistry 37 (1998) 10211–10222.
[11] C. Bakolitsa, J.M. de Pereda, C.R. Bagshaw, D.R. Critchley, R.C. Liddington, Crystal structure of the vinculin tail suggests a pathway for activation, Cell 99 (1999) 603–613.
[12] R.M. Saunders, M.R. Holt, L. Jennings, D.H. Sutton, I.L. Barsukov, A. Bobkov, R.C. Liddington, E.A. Adamson, G.A. Dunn, D.R. Critchley, Role of vinculin in regulating focal adhesion turnover, Eur. J. Cell Biol. 85 (2006) 487–500.
[13] R.P. Johnson, S.W. Craig, An intramolecular association between the head and tail domains of vinculin modulates talin binding, J. Biol. Chem. 269 (1994) 12611–12619.
[14] H. Chen, D.M. Cohen, D.M. Choudhury, N. Kioka, S.W. Craig, Spatial distribution and functional significance of activated vinculin in living cells, J. Cell Biol. 169 (2005) 459–470.
[15] W.H. Ziegler, R.C. Liddington, D.R. Critchley, The structure and regulation of vinculin, Trends Cell Biol. 16 (2006) 453–460.
[16] A.P. Gilmore, K. Burridge, Regulation of vinculin binding to talin and actin by phosphatidyl-inositol-4-5-bisphosphate, Nature 381 (1996) 531–535.
[17] P.A. Steimle, J.D. Hoffert, N.B. Adey, S.W. Craig, Polyphosphoinositides inhibit the interaction of vinculin with actin filaments, J. Biol. Chem. 274 (1999) 18414–18420.
[18] M. Tempel, W.H. Goldmann, G. Isenberg, E. Sackmann, Interaction of the 47-kDa talin fragment and the 32-kDa vinculin fragment with acidic phospholipids: a computer analysis, Biophys. J. 69 (1995) 228–241.
[19] D. Van Der Spoel, E. Lindahl, B. Hess, G. Groenhof, A.E. Mark, H.J.C. Berendsen, GROMACS: fast, flexible, and free, J. Comput. Chem. 26 (2005) 1701–1718.
[20] H.J.C. Berendsen, J.P.M. Postma, W.F. van Gunsteren, J. Hermans, Interaction models for water in relation to protein hydration, in: B. Pullman (Ed.), Intermolecular Forces, Reidel, Dordrecht, 1981.
[21] C. Oostenbrink, T.A. Soares, N.F. van der Vegt, W.F. van Gunsteren, Validation of the 53A6 GROMOS force field, Eur. Biophys. J. 34 (2005) 273–284.
[22] B. Hess, H. Bekker, H.J.C. Berendsen, J.G.E.M. Fraaije, LINCS: a linear constraint solver for molecular simulations, J. Comput. Chem. 18 (1997) 1463–1472.
[23] H.J.C. Berendsen, J.P.M. Postma, W.F. Van Gunsteren, A. DiNola, J.R. Haak, Molecular dynamics with coupling to an external bath, J. Chem. Phys. 81 (1984) 3684–3690.
[24] W. Kabsch, C. Sander, Dictionary of protein secondary structure: pattern recognition of hydrogen-bonded and geometrical features, Biopolymers 22 (1983) 2577–2637.
[25] J.H. Ward, Hierarchical grouping for evaluating clustering methods, J. Am. Stat. Assoc. 58 (1963) 236–244.
[26] R. Mojena, Hierarchical grouping methods and stopping rules: an evaluation, Comput. J. 20 (1977) 359–363.
[27] A. Lobley, L. Whitmore, B.A. Wallace, DICHROWEB: an interactive website for the analysis of protein secondary structure from circular dichroism spectra, Bioinformatics 18 (2002) 211–212.
[28] L. Whitmore, B.A. Wallace, DICHROWEB, an online server for protein secondary structure analyses from circular dichroism spectroscopic data, Nucleic Acids Res. 32 (2004) W668–W673.
[29] M. Tempel, W.H. Goldmann, C. Dietrich, V. Niggli, T. Weber, E. Sackmann, G. Isenberg, Insertion of filamin into lipid membranes examined by calorimetry, the film balance technique, and lipid photolabeling, Biochemistry 33 (1994) 12565–12572.
[30] I. Chandrasekar, T.E. Stradal, M.R. Holt, F. Entschladen, B.M. Jockusch, W.H. Ziegler, Vinculin acts as a sensor in lipid regulation of adhesion-site turnover, J. Cell Sci. 118 (2005) 1461–1472.
[31] C. Bakolitsa, D.M. Cohen, L.A. Bankston, A.A. Bobkov, G.W. Cadwell, L. Jennings, D.R. Critchley, S.W. Craig, R.C. Liddington, Structural basis for vinculin activation at sites of cell adhesion, Nature 430 (2004) 583–586.
[32] L. Whitmore, B.A. Wallace, Protein secondary structure analyses from circular dichroism spectroscopy: methods and reference databases, Biopolymers 89 (2008) 392–400.